Supplementary information for:

Cadmium sulphide quantum dots with tunable electronic properties by bacterial precipitation

K. E. Marusak,[a] Y. Feng,[a] C. F. Eben,[b] S. T. Payne,[b] Y. Cao,[b] L. You,[b] and S. Zauscher[a]*

[a]Department of Mechanical Engineering & Materials Science and , 144 Hudson Hall, Box 90300 Durham, NC 27708, United States. E-mail: zauscher@duke.edu

[b]Department of Biomedical Engineering, Duke University, 101 Science Drive, Durham NC 27708, United States

1. Control image of bacterial cultures

To demonstrate that all three ingredients, *E. coli*, cysteine, and $CdCl_2$, are necessary for CdS precipitation, we conducted a control experiment. Fig. S1 shows four culture tubes each containing modified M9 media, carbenicillin, K_2SO_4, and IPTG. Additional ingredients in each tube are indicated in the image. The leftmost culture tube contained all necessary precursors for particle precipitation (cysteine and $CdCl_2$) but did not contain *E. coli*. The absence of yellow precipitate suggests that cysteine does not directly interact with Cd ions in solution and that the presence of *E. coli* is necessary for particle precipitation. The presence of *E. coli* in suspension causes the "cloudy" nature of the cultures. The next culture tube (second from the left) contains *E. coli* and $CdCl_2$, but does not contain supplemental cysteine, the sulphur source. While there may be natural cysteine within the system, the amount is negligibly small, especially considering that an excess of cysteine is used in our precipitation experiments. The next culture tube (third from the left) contains *E. coli* and cysteine, but does not contain $CdCl_2$. Without any cadmium source there is no potential for CdS precipitation. Additionally, increased bacterial growth is observed (we qualitatively notice denser media) due to a lack of cadmium ions that can be toxic to the bacteria at high doses. Finally, the rightmost culture tube contains $CdCl_2$, cysteine, and *E. coli* and clearly shows the presence of a yellow precipitate that, as we have previously shown, contains CdS.

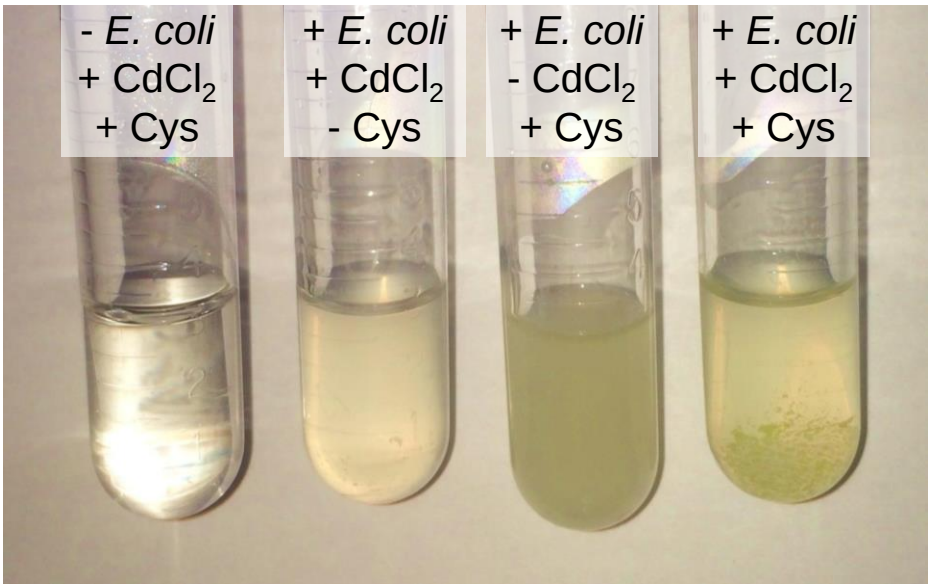

Fig. S1 Digital image of culture tubes containing culture media, K_2SO_4, and IPTG. From the left, in tubes 1, 2 and 3 one ingredient necessary for CdS NP precipitation (*E. coli*, cysteine, and $CdCl_2$, from left to right) is missing. The rightmost tube contains all ingredients and shows yellow precipitation indicative of CdS. The other cultures did not display this yellow precipitate.

2. UV-vis for bandgap calculation

a. Example determination of absorption onset and calculation of bandgap

The onset of the absorption is determined by linear extrapolation of the baseline and the absorption edge. The intercept is then used in Planck's relation (upper right Fig. S2) to determine the average bandgap energy. This bandgap energy is then also used to calculate the crystallite size (Fig. 5).

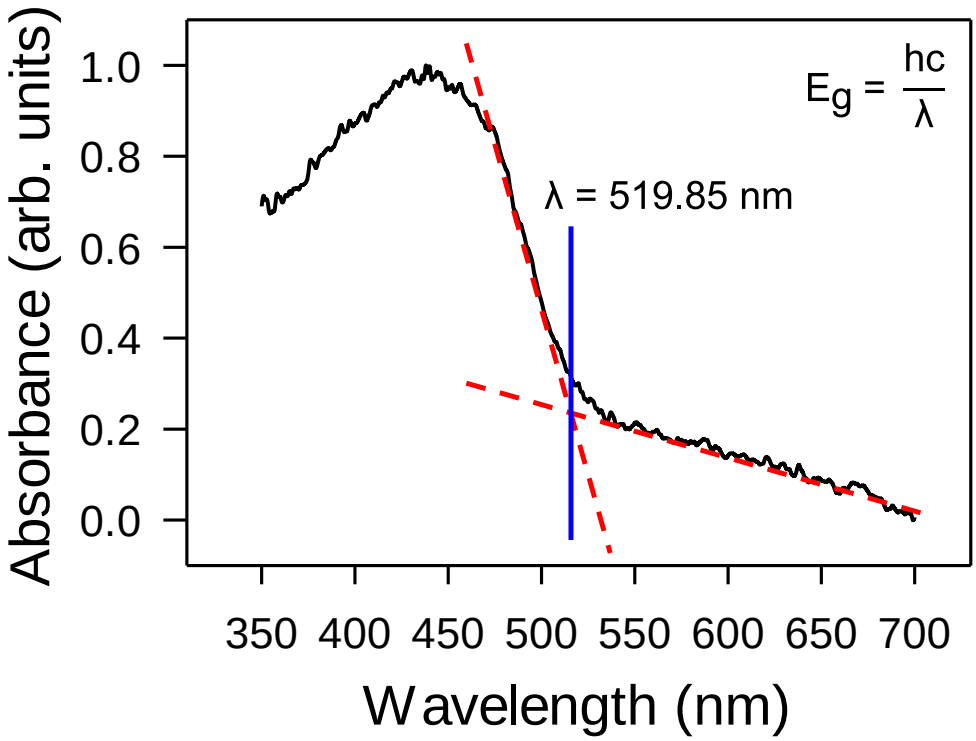

Fig. S2 Example showing the calculation of the bandgap energy from the UV-vis absorption spectrum. The spectrum shown is for bacterially precipitated NPs extracted from the 0.4 mM $CdCl_2$ sample shown in the top, rightmost image of Fig. 3 and Fig. S10).

b. Representative UV-vis spectra of samples in Fig. S10

The bandgap energies of the samples and the crystallite diameters derived from them are determined by analyzing multiple, normalized UV-vis spectra for each sample and averaging

the values for the onset of the absorption. A representative spectrum of each sample is shown in Fig. S3.

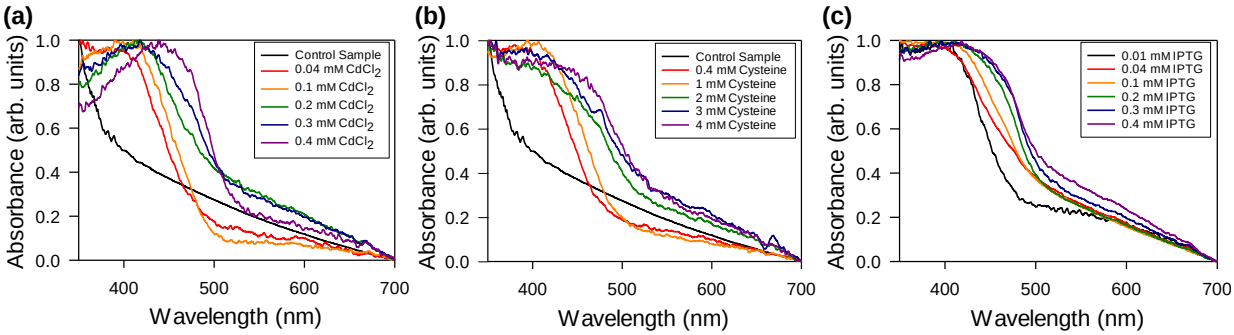

Fig. S3 Representative UV-vis spectra of CdS NP thin film samples shown in Fig. 3.

3. Transient photocurrent responses

CdS is a direct, wide-bandgap semiconductor, making it a photoactive material.[1] When irradiated with visible light, CdS generates charge carriers which can be accumulated at electrodes before recombination. This accumulation creates a voltage that can drive chemical reactions such as water splitting.[2]

a. Photoelectrochemical testing

The transient photocurrent reflects both the photoactivity of the CdS and the internal series-resistance of the photoelectrochemical cell. Briefly, a three electrode system was used (Fig. S4). The working electrode was connected to the electrochemical workstation via a copper wire, which was isolated from the electrolyte by a glass tube and epoxy (not shown). The counter electrode (CE) was a 2.5 cm long platinum wire with a diameter of 0.5 mm, the reference electrode (RE) was Ag/AgCl, and the electrolyte was 0.5 M sodium sulphate (Na_2SO_4) aqueous solution. A + 0.5 V bias voltage (*vs.* Ag/AgCl) was applied upon repeated exposure and shielding of the sample from light. The photocurrent density *vs.* time plot is shown in Fig. 7.

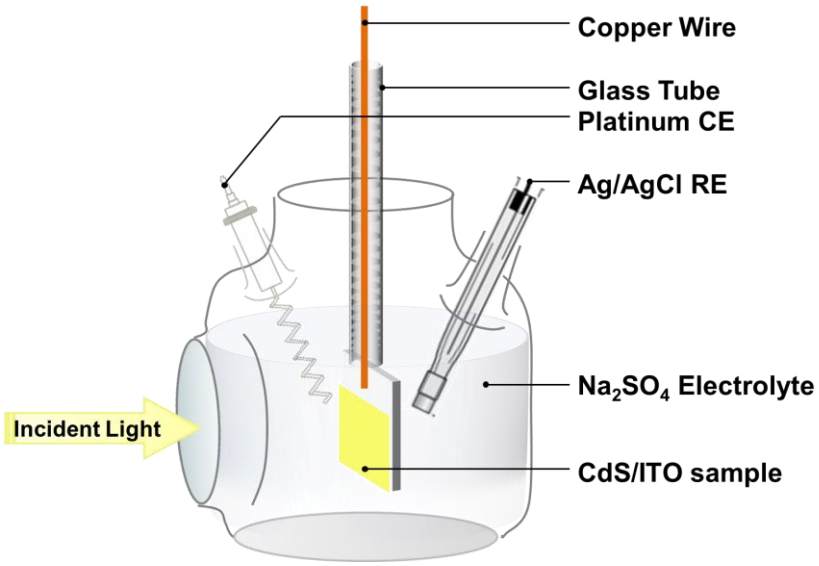

Fig. S4 Experimental set-up used for measuring the transient photocurrent response of bacterially synthesized CdS NPs. The three-electrode electrochemistry cell was connected to an electrochemistry work station to detect the photoactivity of CdS NP thin films coated onto ITO covered glass slides. The incident light enters the cell through a planar quartz window. CE stands for counter electrode and RE stands for reference electrode.

b. The band diagram of the CdS-electrolyte interface under different conditions

In Fig. S5a-d, the left half represents the CdS, and the right half represents the electrolyte. Most CdS materials are n-doped semiconductors and under equilibrium conditions the conduction band (CB), valence band (VB), and the Fermi energy level (E_f) bend up at the interface with the electrolyte to match the electron energy level in the electrolyte (solid line at right in Fig. S5a).[3] When a + 0.5 V (*vs.* Ag/AgCl) the band bending increases due to a potential difference generated between the chemical potential of the reference electrode and the electron energy level in the electrolyte which aligns with the E_f of CdS, as shown in Fig.S5b. When this system is irradiated with light, electrons and holes are generated. This causes an increase in the charge carrier density in CdS, leading to a photocurrent response that triggers

oxidative reactions in the organic matrix at the interface (Fig. S5c). When the light is blocked from the sample, the electrons and holes recombine in CdS, and, as shown in Fig. 7, a quick drop in current density ensues. After a short period of time, the holes accumulate at the CdS-electrolyte interface and some oxidative reactions can still occur. This causes the local E_f to shift down towards the VB, leading to further upward bending of the CB, blocking the injection of the electrons from the electrolyte, which is shown in Fig. S5d. This blocking effect slows the recombination rate in CdS by leaving higher probabilities for holes to react, and is reflected as a reduced current density drop rate. Many factors may cause the accumulation of holes at the CdS-electrolyte surface, such as the blocking effect from the porous, less conductive, organic matrix; the trapping effect from some reductive reagents from the organic matrix; or the transfer energy barrier caused by grain boundaries due to the small CdS crystalline size.[3] We note that while we controlled for overall CdS concentration, we were not able to keep consistent the layer thickness between the two experiments owing to the less-pure nature of the bacterially precipitated CdS. Additionally, we did not control particle size in the CBD system which can affect the overall photoelectrochemical properties of the device.

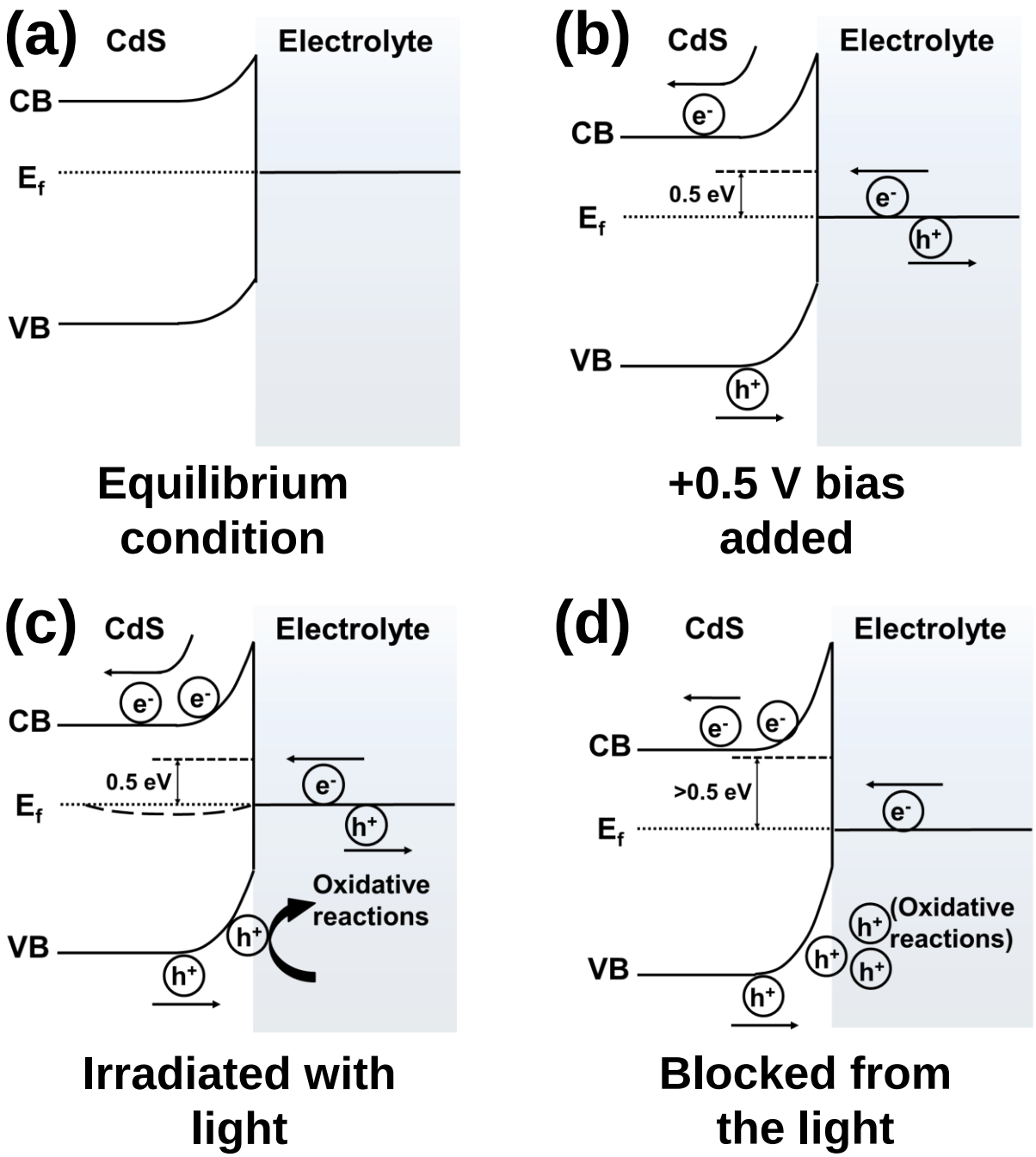

Fig. S5 Schematic, showing the band diagram of the CdS-electrolyte interface under different conditions. (a) Under equilibrium condition (b) under + 0.5 V (*vs.* Ag/AgCl) bias (c) under light irradiation with the same bias, and (d) after the light was turned off with the same bias.

4. XPS survey and high resolution oxygen scan of bacterially precipitated CdS NPs

In Fig. 2a in the main text we showed a high resolution scan of the Cd 3d doublet peak of bacterially precipitated CdS NPs extracted from lysed bacteria. Here, for reference, we display the (a) survey scan and the high resolution scan for the (b) oxygen 1s peak (Fig. S6). The survey scan shows, in addition to Cd and S, several strong peaks, associated with C, O, and N most likely from the bacteria, and a series of weak peaks, including P, Ca, Na, and Mg, most likely associated with the elements of the bacterial growth buffer. The survey scan (Fig. S6a) indicates the presence of a small amount (about 2.2 at%) of sulphur on the particle surfaces. The peak position of the sulphur 2p peak is at ~169 eV, *i.e.*, a much higher binding energy than that expected for metal sulphides such as CdS (~161.5 eV). Splitting of the spin-orbit doublet was not observed in the relatively noisy, high resolution spectrum of the sulphur 2p peak (data not shown). These observations are in line with the notion that sulphur is present on the particle surfaces largely as thiosulphate, and only a very small amount of sulphur is bound to Cd. The deconvolution of the robust, high resolution oxygen 1s peak (Fig. S6b) supports the observed (Fig. 2a) predominant bonding of Cd on the particle surface to oxygen (~0.6 at%, *i.e.*, 30.6 at% x 2%, from peak deconvolution), in good agreement with the binding percentage (0.7 at%, *i.e.*, 1.1 at% x 62%) derived from the deconvolution of the Cd 3d peak.

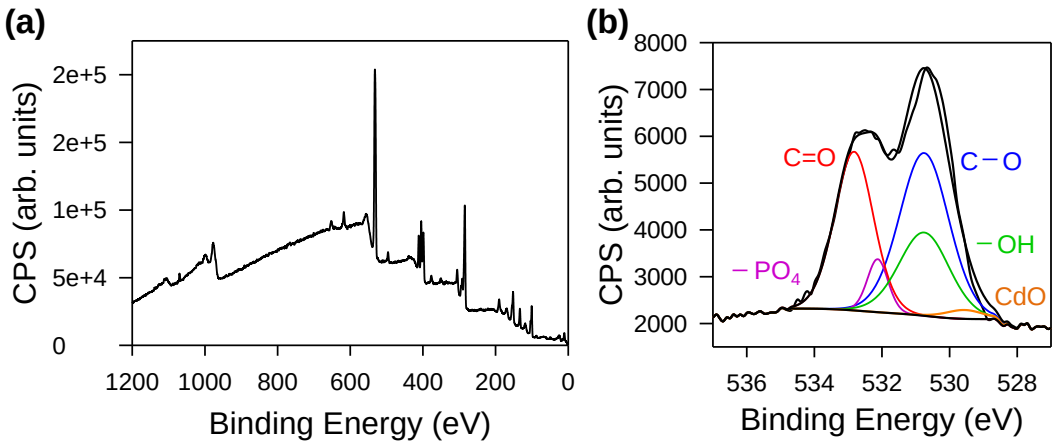

Fig. S6 (a) XPS survey scan and high resolution scan of the (b) 1s oxygen peak from bacterially precipitated CdS NPs extracted by lysing bacteria. The colored lines in (b) display the deconvolution of the oxygen peak.

5. Selected XRD reference patterns

To confirm the crystal structure of our bacterially precipitated CdS, we compare our XRD spectrum with reference spectra of other, potential cadmium compounds (Fig. S7). Since CdS occurs often in two crystalline habits (fcc and hcp), we include here the spectra for both hcp and fcc CdS (PDF nos. 00-041-1094 and 01-089-0440, respectively). As seen in Fig. S7, the peaks in our XRD data are quite broad so that a unique assignment to fcc is not possible, particularly considering that the peak positions for hcp and fcc are, in places, very close, and considering that CdS often occurs as a mixture of both crystal habits. Comparing with the spectrum for $CdCl_2$ (PDF no. 00-009-0401) one sees that there is sufficient mismatch that suggests that $CdCl_2$ (our Cd precursor) likely does not contribute to the crystalline makeup of the sample. Furthermore, we compare to CdO (PDF no. 00-005-0640) to further support the interpretation of our XPS data (Fig. 2a). We conclude that while there is some surface oxidation of the NPs as

shown by XPS, the XRD data indicate that the sample is still mostly composed of non-oxidized CdS. We also inspected the reference patterns of many other cadmium compounds, not shown here, including phosphates, phosphides, nitrates, nitrides, sulphates, sulphides, carbonates, acetates, and elemental cadmium. In all cases, the major peak positions are sufficiently different from those measured here to exclude any of these compounds as a major constituent of our sample.

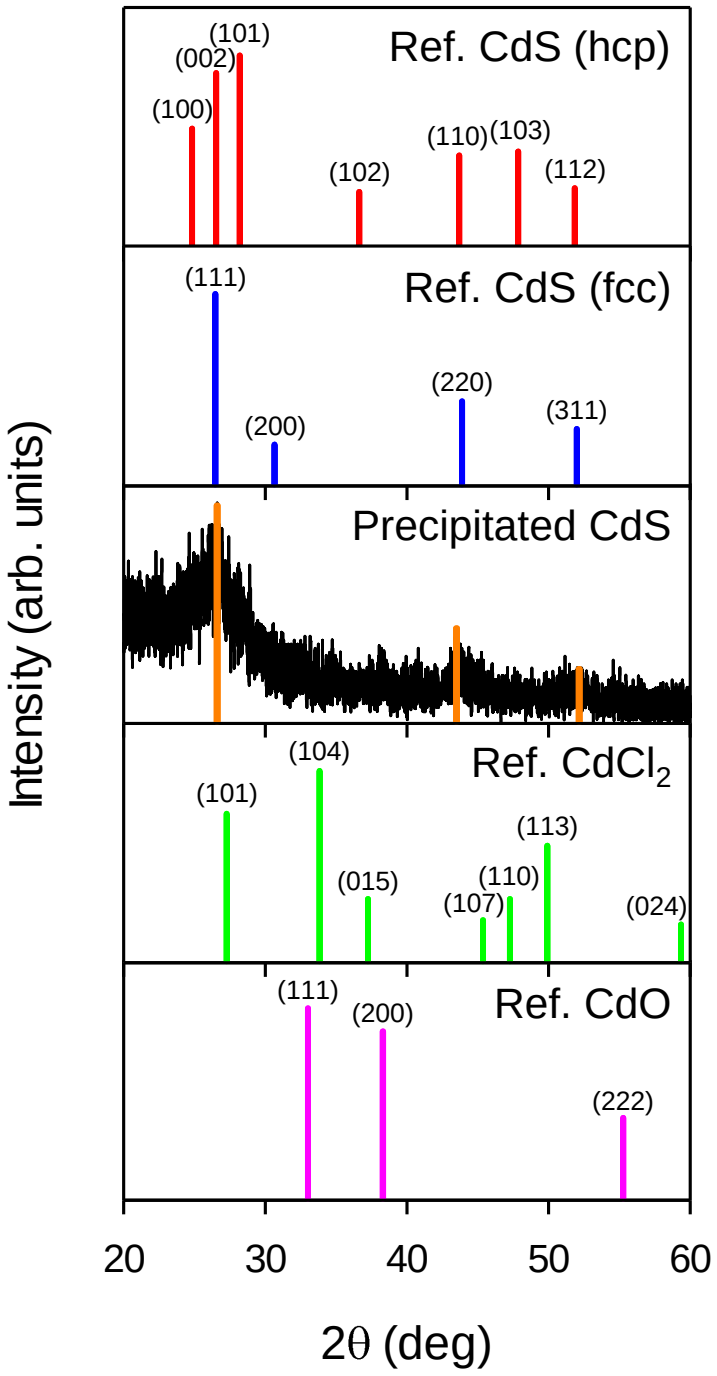

Fig. S7 XRD spectra of selected references and of our bacterially precipitated CdS NP film. Each bar is labeled with its reported Miller indices. Orange bars, overlaid on the measured spectrum, are added to aid in the comparison with the reference spectra. PDF nos. include CdS (hcp): 01-089-0440, CdS (fcc): 00-041-1094, $CdCl_2$: 00-009-0401, and CdO: 00-005-0640.

6. Representative control sample TEM micrograph

CdS NP precipitation requires the presence of precursors in sufficiently high concentrations. Fig. S8 depicts a control sample with no $CdCl_2$, supplemental cysteine, or IPTG added to the culture, and should be considered in conjunction with Fig. 3 in the paper. In contrast to Fig. 3, electron dense NPs, associated with CdS NP precipitates, are not visible in Fig. S8. Fig. S6 is representative of the entire culture and is presented here at a magnification of 25kx, consistent with the magnification of the images shown in Fig. 3 (though the dimensions of the image is not consistent easier examination).

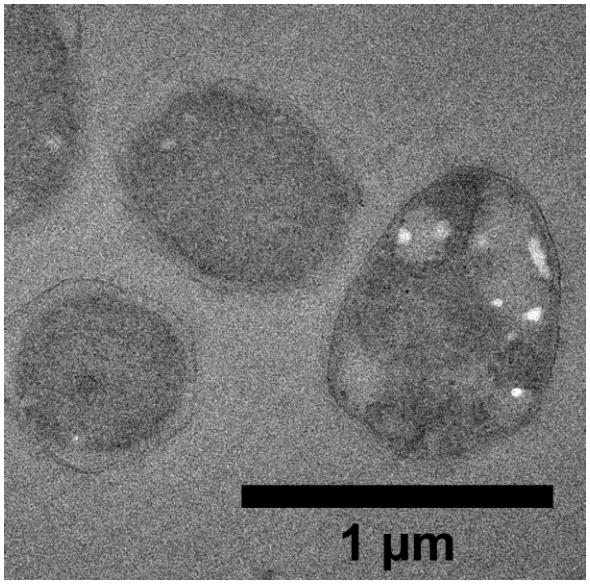

Fig. S8 TEM image of control sample (no $CdCl_2$, supplemental cysteine, or IPTG added) at Mag = 25kx for Fig. 3.

7. Image analysis of NPs by MATLAB

The MATLAB image processing toolbox was used to measure the diameters of precipitated NPs (explained in more detail in the Experimental). Fig. S9 shows that the median NP diameter is relatively independent of the $CdCl_2$ and cysteine precursor concentrations, aside

from an initial increase at very low concentrations. However, there is an increasing range of NP clusters outside the 90th percentile at the high end of the distribution with increasing $CdCl_2$ concentration. This is likely due to the continued nucleation of NPs throughout the bacterial growth phases. The lower bounds are unaffected as they are largely determined by the resolution limit of the technique. There is no apparent trend in NP size with increasing IPTG concentration, consistent with the notion that IPTG acts as an "on/off" promotor for cysteine desulfhydrase production. As mentioned in the main text, the missing data point for the lowest concentration of $CdCl_2$ (0.01 mM) is due to a lack of visible CdS NPs.

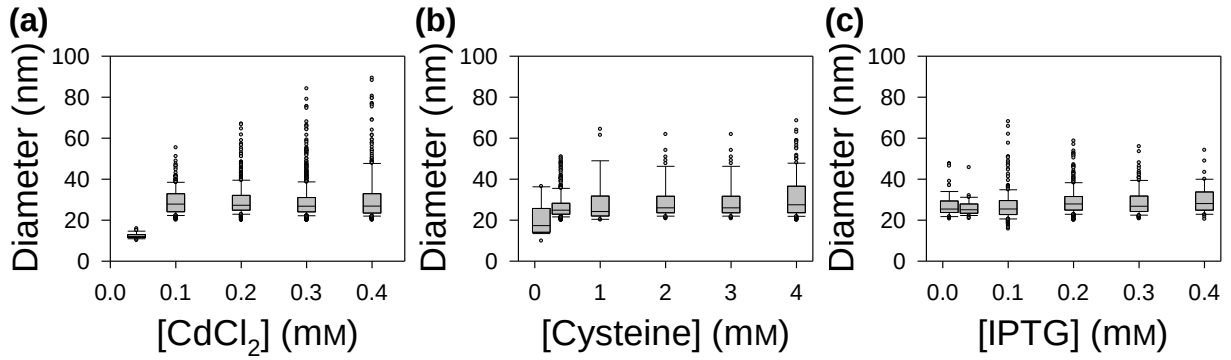

Fig. S9 NP size analysis (using MATLAB code) of samples shown in Fig. 3. Plots show 25th, 50th (median), and 75th percentiles as vertical boxes with the middle lines indicating the median. The whiskers display the 10th and 90th percentiles and outliers of this range are indicated by grey-filled circles.

8. Additional isolated CdS crystallite data

a. Representative high-resolution TEM of samples in Fig. 4

The high-resolution (Mag = 700kx) TEM micrographs in Fig. S10 show crystallites with lattice, with the exception of the sample at the lowest $CdCl_2$ concentration. Although some crystallites likely also grew in this sample, the amounts were too small to be clearly visible in

TEM. The examples of crystallites shown in Fig. S10 are representative of those seen in the sample populations. The corresponding, manually measured crystallite diameters are summarized in Fig. 4 and S11.

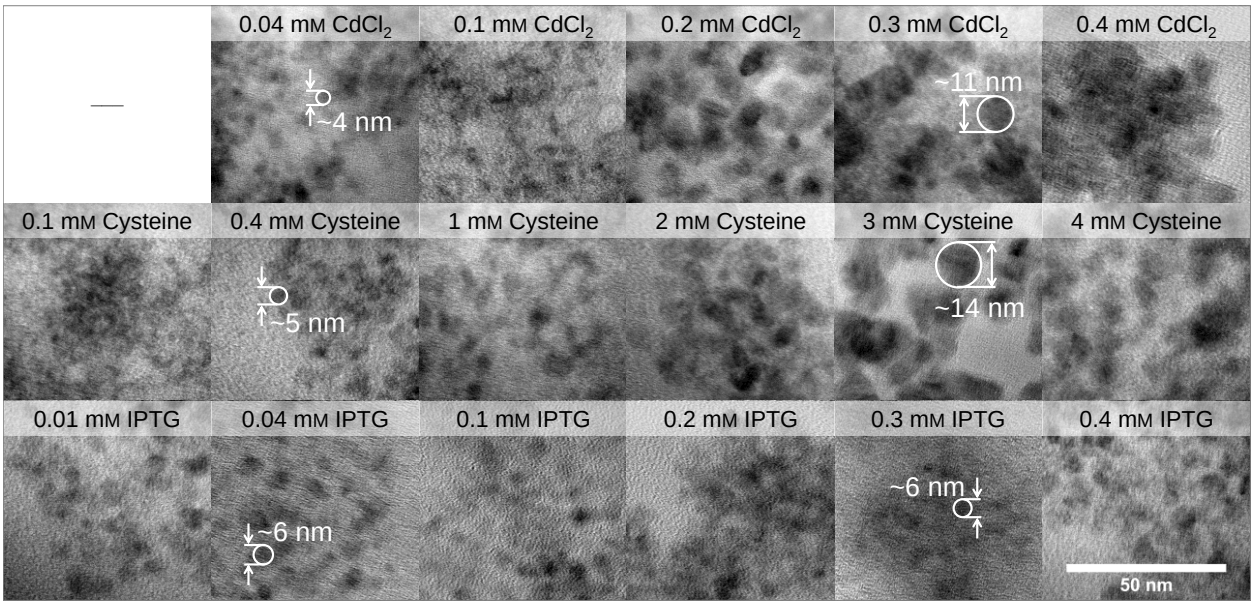

Fig. S10 Representative, high-resolution TEM images of CdS NPs used to show nanocrystal size distributions in Fig. 4. Row 1: Increasing $CdCl_2$ concentrations with 0.1 mM IPTG and 1 mM cysteine in each. Row 2: Increasing cysteine concentrations with 0.1 mM $CdCl_2$ and 0.1 mM IPTG in each. Row 3: Increasing IPTG concentrations with 0.1 mM $CdCl_2$ and 1 mM cysteine in each. (Mag = 700kx) Circles in the TEM images indicate representative crystallites.

b. Box plots of size distribution of manually measured NP diameters

In addition to histograms shown in Fig. 4, we show here also box plots the of the manually measured diameter distributions of isolated, bacterially precipitated CdS crystallites. The data show that crystallite size strongly depends on $CdCl_2$ and cysteine concentrations, and not on IPTG concentration. We also note that the size of precipitates outside the 90th percentile (*i.e.*, large outliers) increases with increasing $CdCl_2$ and cysteine concentrations.

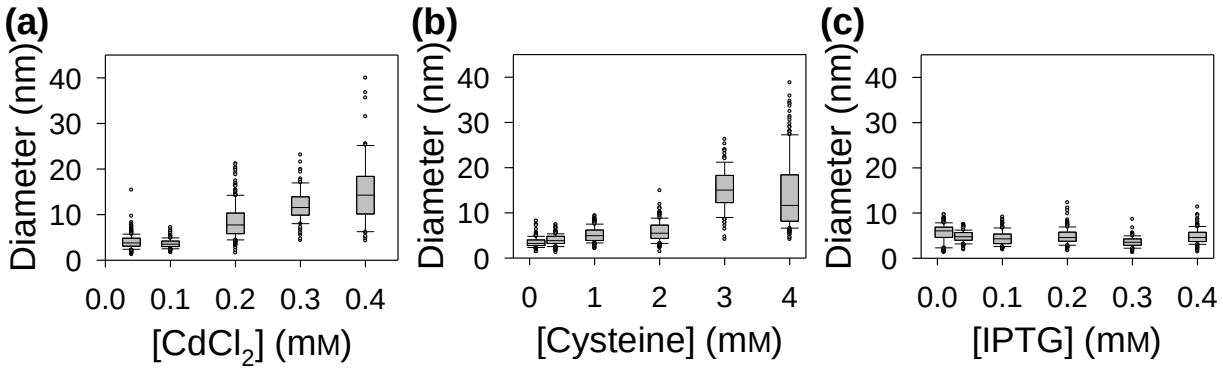

Fig. S11 Manually measured diameter values of isolated CdS crystallites for samples of increasing (a) [$CdCl_2$], (b) [Cysteine], and (c) [IPTG] (Mag = 700kx). Box plots show 25th, 50th (median), and 75th percentiles as vertical boxes with the middle lines indicating the median. The whiskers display the 10th and 90th percentiles, and outliers of this range are indicated by grey-filled circles.

9. Digital image of a litre culture of bacteria with suspended CdS NPs

To show the ability to scale-up the bacterial precipitation system, we grew up a 1 litre culture of our bacteria with $CdCl_2$ (Fig. S12). We were able to harvest and purify the particles and are now using them for further experiments. Additionally, in the sample shown in Fig. S12, we used a higher $CdCl_2$ concentration (0.2 mM of $CdCl_2$ rather than 0.1 mM, used previously), and we induced extracellular precipitation (example Fig. 6b) to aid in particle extraction.

Fig. S12 Digital image of a 1 litre culture of CdS precipitating bacteria, showing the typical yellow color associated with CdS in the culture.

10. Supporting table

Table S1 is a comprehensive summary of all values measured and calculated throughout the paper with standard deviations (propagation of error was performed). Additionally, it allows for easier comparison of the calculated and manually measured crystallite diameters.

Sample	Conc.	Onset [nm]	Std. Dev [nm]	Bandgap [eV]	Std. Dev [eV]	Calc. Diam. [nm]	Std. Dev. [nm]	Meas. Diam. [nm]	Std. Dev. [nm]
Control	-	375.1	-	-	-	-	-	-	-
$CdCl_2$	0.01 mM	389.2	3.0	3.19	0.02	3.17	0.02	-	-
	0.04 mM	472.0	4.2	2.63	0.02	5.07	0.09	4.0	1.5
	0.1 mM	487.0	5.2	2.55	0.03	5.86	0.16	3.7	1.0
	0.2 mM	499.0	4.7	2.49	0.02	6.83	0.23	8.5	3.8
	0.3 mM	517.7	1.1	2.40	0.01	10.47	0.25	12.1	3.6
	0.4 mM	518.4	1.6	2.39	0.01	10.84	0.40	15.1	7.4
Cysteine	0.1 mM	406.6	7.9	3.05	0.06	3.43	0.06	3.4	1.1
	0.4 mM	476.7	1.6	2.60	0.01	5.28	0.04	4.0	1.1
	1 mM	486.1	5.7	2.56	0.03	5.80	0.17	5.2	1.6
	2 mM	509.6	5.7	2.44	0.03	8.43	0.47	5.9	2.2
	3 mM	516.3	6.1	2.40	0.03	11.55	1.08	15.2	4.5
	4 mM	523.0	0.9	2.36	0.01	15.63	0.89	14.2	7.9
IPTG	0.01 mM	464.1	2.4	2.67	0.01	4.71	0.04	5.7	1.9
	0.04 mM	479.3	3.1	2.59	0.02	5.41	0.08	4.8	1.2
	0.1 mM	499.7	6.5	2.48	0.03	6.93	0.33	4.5	1.5
	0.2 mM	506.7	5.5	2.45	0.03	7.84	0.41	4.9	1.7
	0.3 mM	505.5	3.7	2.45	0.02	7.59	0.26	3.6	1.1
	0.4 mM	506.3	8.9	2.45	0.04	8.16	0.65	4.9	1.6

Table 1 Comprehensive summary of all values measured and calculated throughout the paper with standard deviations.

References

1 P. E. Lippens and M. Lannoo, *Phys. Rev. B*, 1989, **39**, 10935–10942.

2 G. Wang, X. Yang, F. Qian, J. Z. Zhang and Y. Li, *Nano Lett.*, 2010, **10**, 1088–1092.

3 J. C. Moore and C. V Thompson, *Sensors*, 2013, **13**, 9921–9940.